

1 **Direct observations indicate photodegradable oxygenated VOCs**  
2 **as larger contributors to radicals and ozone production in the**  
3 **atmosphere**

4 Wenjie Wang<sup>1,2</sup>, Bin Yuan<sup>1,3\*</sup>, Yuwen Peng<sup>1,3</sup>, Hang Su<sup>2\*</sup>, Yafang Cheng<sup>2</sup>, Suxia Yang<sup>1,3</sup>,  
5 Caihong Wu<sup>1,3</sup>, Jipeng Qi<sup>1,3</sup>, Fengxia Bao<sup>2</sup>, Yibo Huangfu<sup>1,3</sup>, Chaomin Wang<sup>1,3</sup>,  
6 Chenshuo Ye<sup>1</sup>, Zelong Wang<sup>1,3</sup>, Baolin Wang<sup>4</sup>, Xinming Wang<sup>5</sup>, Wei Song<sup>5</sup>, Weiwei  
7 Hu<sup>5</sup>, Peng Cheng<sup>6</sup>, Manni Zhu<sup>1,3</sup>, Junyu Zheng<sup>1,3</sup>, Min Shao<sup>1,3</sup>

8  
9 <sup>1</sup> Institute for Environmental and Climate Research, Jinan University,  
10 Guangzhou 511443, China

11 <sup>2</sup> Multiphase Chemistry Department, Max Planck Institute for Chemistry, Mainz  
12 55128, Germany.

13 <sup>3</sup> Guangdong-Hongkong-Macau Joint Laboratory of Collaborative Innovation for  
14 Environmental Quality, Guangzhou, 511443, China

15 <sup>4</sup> School of Environmental Science and Engineering, Qilu University of  
16 Technology, Jinan 250353, China

17 <sup>5</sup> State Key Laboratory of Organic Geochemistry, Guangzhou Institute of  
18 Geochemistry, Chinese Academy of Sciences, Guangzhou 510640, China

19 <sup>6</sup> Institute of Mass Spectrometry and Atmospheric Environment, Jinan  
20 University, Guangzhou 510632, China

21

22 *\*Correspondence to:* Bin Yuan ([byuan@jnu.edu.cn](mailto:byuan@jnu.edu.cn)); Hang Su ([h.su@mpic.de](mailto:h.su@mpic.de))

23

24

25 **Abstract:** Volatile organic compounds (VOCs) regulate atmospheric oxidation capacity,  
26 and the reactions of VOCs are key in understanding ozone formation and its mitigation  
27 strategies. When evaluating its impact, most previous studies did not fully consider the  
28 role of oxygenated VOCs due to limitations of measurement technology. By using a  
29 proton-transfer-reaction time-of-flight mass spectrometer (PTR-ToF-MS) combined  
30 with gas chromatography mass spectrometer (GC-MS) technology, a large number of  
31 oxygenated VOCs have been quantified in Guangzhou city, China.~~we are able to~~  
32 ~~quantify a large number of oxygenated VOCs in a representative urban environment in~~  
33 ~~southern China.~~ Based on the new dataset, ~~we find that non-formaldehyde (HCHO)~~  
34 ~~OVOCs can contribute large fractions (22-44%) of total RO<sub>x</sub> radical production,~~  
35 ~~comparable or larger than the contributions from nitrous acid and formaldehyde.~~ We  
36 demonstrate that constraints using OVOCs observations are essential in modeling  
37 radical and ozone production, as modelled OVOCs can be substantially lower than  
38 measurements, potentially due to primary emissions and/or missing secondary sources.  
39 Non-formaldehyde (HCHO) OVOCs can contribute to large fractions (22-44%) of total  
40 RO<sub>x</sub> radical production, which is comparable to or larger than the contributions from  
41 nitrous acid and formaldehyde. Our results show that models without OVOC  
42 constraints using ambient measurements will underestimate the production rates of  
43 RO<sub>x</sub> and ozone~~production rate~~, and may also affect the determination of sensitivity  
44 regime in ozone formation. Therefore, a thorough quantification of photodegradable  
45 OVOCs species is in urgent need to understand accurately the ozone chemistry and to  
46 develop effective control strategies.

47  
48 **Keywords:** photolysis reactions; oxygenated volatile organic compounds; radical  
49 production; ozone production

50

## 51 **1 Introduction**

52 Ground-level ozone is generated by photochemical oxidation of volatile organic  
53 compounds (VOCs) under the catalysis of nitrogen oxides (NO<sub>x</sub>) and hydrogen  
54 oxidehydroxide radicals (HO<sub>x</sub>=OH+HO<sub>2</sub>) (Atkinson, 2000;Monks et al., 2015). In  
55 this process, photolysis reactions are a crucial driving force. ~~Photodegradable species—~~  
56 ~~(i.e. species that is capable of photolysis) including~~Photolysis of O<sub>3</sub>, nitrous acid  
57 (HONO), and oxygenated VOCs (OVOCs) can contribute to primary production of  
58 RO<sub>x</sub> (OH+HO<sub>2</sub>+RO<sub>2</sub>) radicals ~~via photolysis reactions~~, thereby accelerating the  
59 recycling of radicals to generate ozone (Volkamer et al., 2010). The strong  
60 dependence of OH concentration on j(O<sup>1</sup>D) was found in a number of field  
61 measurements (Ehhalt and Rohrer, 2000;Rohrer et al., 2014b;Stone et al., 2012),  
62 implying the dominant role of ultraviolet radiation and photolysis reactions in the  
63 production of HO<sub>x</sub> radicals. Edwards et al. (2014) found that the high ozone pollution  
64 in an oil and gas producing basin in the U.S. in winter was caused by the photolysis of  
65 high concentrations of OVOCs to generate sufficient oxidants. A recent model  
66 simulation with limited OVOCs measurements by Qu et al.(Qu et al., 2021) indicated  
67 that OVOC species is the largest free-radical source in the boundary layer. Another  
68 study indicated that fast ozone production during winter haze episodes in China was  
69 driven by HO<sub>x</sub> radicals derived from photolysis of formaldehyde (HCHO),  
70 overcoming radical titration induced by NO<sub>x</sub> emissions (Li et al., 2021). Therefore, an  
71 accurate quantification of numerous photolysis reactions is necessary to understand  
72 the mechanism of RO<sub>x</sub> radical and ozone production.

73 However, only limited number of photodegradable OVOCs species, such as  
74 formaldehyde, acetaldehyde and acetone, have been measured in the field campaigns  
75 in China due to the limitations of measurement technology (Lu et al., 2013;Lu et al.,  
76 2012;Tan et al., 2018;Tan et al., 2019c). Many important photodegradable OVOCs,  
77 such as larger aldehydes and ketones, carboxylic acids, nitrophenols, organic peroxides  
78 and multifunctional species, have been rarely quantified accurately in ambient  
79 environments. In such cases, the quantification of the primary production of RO<sub>x</sub>

80 radicals induced by photolysis reactions may not be adequately accurate. Many studies  
81 used photochemical models to simulate unmeasured OVOC species (Tan et al.,  
82 2019b; Volkamer et al., 2010; Ling et al., 2014; Edwards et al., 2014). However, large  
83 uncertainties in the simulation of OVOCs remain due to primary emissions of OVOCs  
84 (McDonald et al., 2018; Karl et al., 2018; Gkatzelis et al., 2021), missing secondary  
85 sources (Bloss et al., 2005; Ji et al., 2017), heterogenous uptake of aerosols and  
86 unknown dilution and transmission processes (Li et al., 2014). For instance, chamber  
87 experiments of the oxidation of aromatics by OH radical indicated that MCM  
88 mechanism generally underestimated the formation of aldehydes, ketones and phenols  
89 by 10-70% (Bloss et al., 2005; Ji et al., 2017), implying the existence of unknown  
90 production pathways for these OVOC species. Furthermore, model simulations  
91 frequently underestimated observed RO<sub>x</sub> radicals in ambient studies of RO<sub>x</sub> radicals  
92 (Hofzumahaus et al., 2009; Tan et al., 2018; Lelieveld et al., 2008; Rohrer et al.,  
93 2014a; Sheehy et al., 2010; Emmerson et al., 2005; Ma et al., 2019). Given that only  
94 limited photodegradable OVOCs species were measured in these studies, the lack of  
95 comprehensive measurements of OVOCs to constrain the model is likely to be a cause  
96 of the underestimation.

97 Thus far, the concrete effects of photodegradable OVOCs on radical and ozone  
98 production remains unexplored in China. Based on comprehensive field observations  
99 in a mega-city in southern China, a variety of important photodegradable OVOC  
100 species were measured. The contributions of these photodegradable OVOCs species  
101 to the production of RO<sub>x</sub> radicals are quantified, and the effect of photolysis reactions  
102 on ozone production is quantitatively assessed.

## 103 **2 Materials and Methods**

### 104 **2.1 OVOC measurements**

105 Field measurements were conducted at an urban site in Guangzhou (113.2°E, 23°N)  
106 from 14 September to 20 November 2018. The sampling site is located on the 9th floor  
107 of a building on the campus of Guangzhou Institute of Geochemistry, Chinese Academy

108 of Sciences, 25 m above the ground level. This site is regarded as a typical urban site  
109 in Guangzhou influenced by industrial and vehicle emissions.

110 During this campaign, an online PTR-ToF-MS (Ionicon Analytic GmbH,  
111 Innsbruck, Austria) with  $\text{H}_3\text{O}^+$  and  $\text{NO}^+$  chemistry was used to measure ambient volatile  
112 organic compounds (VOCs) (Wang et al., 2020a; Wu et al., 2020). The PTR-ToF-MS  
113 automatically switches between  $\text{H}_3\text{O}^+$  and  $\text{NO}^+$  modes every 10-20 minutes. In each  
114 mode, the background and ambient measurements were automatically switched to a  
115 custom-built Platinum catalytic converter heated to 365 °C for 3 minutes to detect  
116 background of the instrument. The time resolution of the measurement of PTR-ToF -  
117 MS was 10 s. A total of 31 VOCs species were calibrated using either gas cylinders or  
118 liquid standards. For other measured VOCs, we used the method proposed by Sekimoto  
119 et al. (2017) to determine the relationship between VOC sensitivity and kinetic rate  
120 constants for proton transfer reactions of  $\text{H}_3\text{O}^+$  with VOCs. The fitted line was used to  
121 determine the concentrations of those uncalibrated species. Following the discussions  
122 in Sekimoto, et al. (Sekimoto et al., 2017), the uncertainties of the concentrations for  
123 uncalibrated species were about 50 %. Humidity dependencies of various VOCs were  
124 determined in the laboratory with absolute humidity in the range of 0–30 mmol/mol  
125 (relative humidity of 0 %–92 % at 25 °C), which fully covered the humidity range  
126 encountered during the entire campaign. The detailed introduction of this method has  
127 been reported by Wu et al. (Wu et al., 2020).

128 Notably, PTR-ToF-MS is not capable of distinguishing isomers (Yuan et al., 2017).  
129 GC-MS technique was used to measure several carbonyls that PTR-ToF-MS can not  
130 distinguish, including acetaldehyde, propionaldehyde, n-butanal, n-pentanal, n-hexanal,  
131 methacrolein (MACR), methyl vinyl ketone (MVK). We compared concentrations of  
132 common OVOC species measured by both GC-MS and PTR-ToF-MS. The agreement  
133 of measurement results from the two instruments are quite consistent (Figure S1). In  
134 addition to GC-MS/FID, an iodide time-of flight chemical ionization mass spectrometer  
135 (ToF-CIMS) was used to measure propionic acid. Combined with the measurements of  
136 GC-MS and CIMS, the isomers measured by PTR-ToF-MS can be distinguished. In  
137 OVOC species, hydroxyacetone and propionic acid ( $\text{C}_3\text{H}_6\text{O}_2$ ), acetone and propanal

138 (C<sub>3</sub>H<sub>6</sub>O), methyl ethyl ketone and butanal (C<sub>4</sub>H<sub>8</sub>O), MVK and MACR (C<sub>4</sub>H<sub>6</sub>O) are all  
139 isomers. The average concentration of propionic acid measured by CIMS was 0.23 ppb,  
140 significantly lower than that of the concentration of C<sub>3</sub>H<sub>6</sub>O<sub>2</sub> measured by PTR-ToF-MS  
141 (~1.5 ppb). The hydroxyacetone concentrations were determined by the difference  
142 between PTR-ToF-MS and CIMS measurements. Meanwhile, the concentration of  
143 ~~propanal~~propionaldehyde (average of 0.35 ppb) and n-butanal (average of 0.17 ppb)  
144 measured by GC-MS were also respectively far lower than the concentration of C<sub>3</sub>H<sub>6</sub>O  
145 (average of 4.4 ppb) and C<sub>4</sub>H<sub>8</sub>O (average of 1.8 ppb) measured by PTR-ToF-MS. The  
146 concentrations of acetone and methyl ethyl ketone were determined by the difference  
147 between PTR-ToF-MS and GC-MS measurements. The concentrations of MVK and  
148 MACR were determined according to C<sub>4</sub>H<sub>6</sub>O concentration measured by PTR-ToF-MS  
149 and the ratio of MVK to MACR measured by GC-MS. In this way, the uncertainty of  
150 PTR-ToF-MS induced by isomers is greatly reduced.

151 Concentrations of CH<sub>4</sub>O<sub>2</sub> and CH<sub>4</sub>O<sub>3</sub> were quantified by PTR-ToF-MS, which  
152 were tentatively attributed to methyl hydroperoxide (CH<sub>3</sub>OOH) and hydroxymethyl  
153 hydroperoxide (HOCH<sub>2</sub>OOH), respectively. ~~Furthermore, we also measured~~  
154 concentrations of several small carbon-number acids, including formic acid, acetic acid,  
155 and propionic acid were measured by PTR-ToF-MS (Figure S1). However, the  
156 photolysis wavelength bands of these species are all less than 260 nm. Given the  
157 sunlight that can reach the ground is generally greater than 290 nm, these small carbon-  
158 number acids cannot photolyze significantly near the ground. An exception is pyruvic  
159 acid which is also a small carbon-number acid but with a wide photolysis band that can  
160 reach 460 nm because of its carbonyl functional group (Horowitz et al., 2001; Mellouki  
161 and Mu, 2003; Berges and Warneck, 1992). Therefore, the photolysis of pyruvic acid  
162 was included in the analysis as it can significantly contribute to the production of RO<sub>x</sub>  
163 radicals.

164 In addition to the specific species mentioned above, PTR-ToF-MS measured  
165 carbonyls with higher carbon number including C<sub>n</sub>H<sub>2n</sub>O (n>5), C<sub>n</sub>H<sub>2n-2</sub>O (n>3), C<sub>n</sub>H<sub>2n-</sub>  
166 <sub>2</sub>O<sub>2</sub> (n>3), C<sub>n</sub>H<sub>2n-4</sub>O<sub>2</sub> (n>3) and C<sub>n</sub>H<sub>2n-4</sub>O<sub>3</sub> (n>3). Apparently, multiple isomers that  
167 can't be distinguished specifically may contribute to these species. The measured

168 photodegradable OVOCs species and their concentrations are summarized in **Table S1**.

## 169 **2.2 Other measurements**

170 HONO was measured by a custom-built LOPAP (L**O**ng Path Absorption  
171 Photometer) based on wet chemical sampling and photometric detection (Yu et al.,  
172 2021). HCHO was measured by a custom-built instrument based on the Hantzsch  
173 reaction and absorption photometry. Total OH reactivity was measured by the  
174 comparative reactivity method (CRM) (Sinha et al., 2008; Wang et al., 2021). In this  
175 method, pyrrole (C<sub>4</sub>H<sub>5</sub>N) was used as the reference substance and was quantified by a  
176 quadrupole PTR-MS (Ionicon Analytic, Austria). Non-methane hydrocarbons  
177 (NMHCs) were measured using a gas chromatography-mass spectrometer/flame  
178 ionization detector (GC-MS/FID) system, coupled with a cryogen-free pre-  
179 concentration device. Nitrogen oxides (NO<sub>x</sub>= NO + NO<sub>2</sub>), ozone (O<sub>3</sub>), sulfur dioxide  
180 (SO<sub>2</sub>) and carbon monoxide (CO) were measured by NO<sub>x</sub> analyzer (Thermo  
181 Scientific, Model 42i), O<sub>3</sub> analyzer (Thermo Scientific, 150 Model 49i), SO<sub>2</sub> analyzer  
182 (Thermo Scientific, Model 43i) and CO analyzer (Thermo Scientific, Model 48i). The  
183 meteorological data, including temperature (T), relative humidity (RH) and wind  
184 speed and direction 160 (WS, WD) were recorded by Vantage Pro2 Weather Station  
185 (Davis Instruments Inc., Vantage Pro2) with the time resolution of 1 min. Photolysis  
186 frequencies including  $j(\text{HONO})$ ,  $j(\text{NO}_2)$ ,  $j(\text{H}_2\text{O}_2)$ ,  $j(\text{HCHO})$  and  $j(\text{O}^1\text{D})$  were  
187 measured by a spectrometer (Focused Photonics Inc., PFS-100).

## 188 **2.3 Observation-based box model**

189 A zero-dimensional box model coupled with the Master Chemical Mechanism  
190 (MCM) v3.3.1 chemical mechanism (Jenkin et al., 2003; Saunders et al., 2003) was  
191 used to simulate RO<sub>x</sub> production and losses, and O<sub>3</sub> production rates during the field  
192 campaign. The model simulation was constrained to the observations of  
193 meteorological parameters, photolysis frequencies, and concentrations of non-  
194 methane hydrocarbons (NMHCs), OVOCs, NO, NO<sub>2</sub>, O<sub>3</sub>, CO, SO<sub>2</sub> and nitrous acid  
195 (HONO). All constraints were averaged to generate a synchronized 1-h time

196 resolution dataset. The model runs were performed in a time-dependent mode with  
 197 time resolution of 1 hour and spin-up of two days. There is no significant difference in  
 198 simulated OH and HO<sub>2</sub> concentrations between 1-hour and 5-minute time resolution  
 199 (Figure S3). A 24-h lifetime was introduced for all simulated species, including  
 200 secondary species and radicals, to approximately simulate dry deposition and other  
 201 losses of these species (Lu et al., 2013; Wang et al., 2020b). ~~This lifetime corresponds~~  
 202 ~~to an assumed deposition velocity of 1.2 cm s<sup>-1</sup> and a well-mixed boundary layer~~  
 203 ~~height of about 1 km.~~ Sensitivity tests show that this assumed physical lossdeposition  
 204 lifetime has a relatively small influence on the reactivity of modeled oxidation  
 205 products, RO<sub>x</sub> radicals and ozone production rates. A 50% change in the physical loss  
 206 lifetime leads to 3%, 6% and 10% changes in OH concentration, HO<sub>2</sub> concentration  
 207 and ozone production rate. The ozone production rate (P(O<sub>3</sub>)) were calculated  
 208 according to E1:

$$209 \quad P(O_3) = k_{HO_2+NO} [HO_2][NO] + \sum_i (k_{RO_2+NO}^i [RO_2^i][NO]) \quad E1$$

210 The production rate of RO<sub>x</sub> radicals (P(RO<sub>x</sub>)) is equal to the sum of the rates at  
 211 which all photodegradable species generate RO<sub>x</sub> radicals through the photolysis  
 212 reactions, as shown in E2.

$$213 \quad P(RO_x) = 2 \times [O_3] \times j(O^1D) \times \theta + [HONO] \times j(HONO) + \sum_i [OVOC_i] \times j_i \times k_i \quad E2$$

214 where  $\theta$  is the fraction of O<sup>1</sup>D from ozone photolysis that reacts with water vapor.  
 215 OVOC<sub>i</sub> represents each OVOCs species,  $j_i$  represents the photolysis frequency of each  
 216 OVOC species, and  $k_i$  represents the number of RO<sub>x</sub> radicals generated from the  
 217 photolysis of each OVOC molecule. For most OVOCs species,  $k_i$  is equal to 2 or 1.

218 The photolysis frequencies of measured photodegradable species were calculated  
 219 based on measured actinic flux combined with absorption cross sections and  
 220 photolysis quantum yields reported in Jet Propulsion Laboratory (JPL) publication  
 221 (Burkholder et al., 2020). Note that absorption cross sections and quantum yields used  
 222 all corresponds to radical formation channel, not including molecule formation  
 223 channel. However, absorption cross sections and photolysis quantum yields for  
 224 nitrophenol and methyl nitrophenol are unavailable from JPL publication. Yuan et al.



225 (2016) have reported that photolysis was the most efficient loss pathway for  
226 nitrophenol in the gas phase. Different values of absorption cross sections and  
227 quantum yields for nitrophenol have been reported (Chen et al., 2011; Sangwan and  
228 Zhu, 2018; Bejan et al., 2006). In this study, we used the values from Chen et al. (Chen  
229 et al., 2011), which can reproduce well the observed concentrations of nitrophenol and  
230 methyl nitrophenol during the measurement period.

231 Absorption cross sections and quantum yields are not available for carbonyls  
232 with large carbon number, and absorption cross sections and quantum yields of  
233 species with similar structure are used as a surrogate, following the method described  
234 in Jenkin et al., (Jenkin et al., 1997) (e.g.  $C_2H_5C(O)CH_3$  is used as a surrogate for  
235 aliphatic ketones with more carbons). Another issue is that carbonyls with large  
236 carbon number ( $C_nH_{2n}O$ ,  $n>5$ ;  $C_nH_{2n-2}O$ ,  $n>3$ ;  $C_nH_{2n-2}O_2$ ,  $n>3$ ;  $C_nH_{2n-4}O_2$ ,  $n>3$ ;  $C_nH_{2n-4}O_3$ ,  $n>3$ ) measured by PTR-ToF-MS may include contributions from multiple  
237 isomers, and the fraction of each individual species cannot be obtained. Hence, each  
238 molecular formula corresponds to multiple molecular structures and thus corresponds  
239 to multiple photolysis frequencies. Here, we calculate the  $P(RO_x)$  of these species in  
240 two scenarios: (1) each molecular formula corresponds to minimum photolysis  
241 frequency of all potential species (e.g. aliphatic ketones); (2) each molecular formula  
242 corresponds to maximum photolysis frequency of all potential species (e.g.  
243 aldehydes). As a result, photolysis frequencies of these carbonyls with large carbon  
244 number were assigned to the ranges of  $1.2 \times 10^{-6} \sim 6.5 \times 10^{-6}$ ,  $1.2 \times 10^{-6} \sim 6.5 \times 10^{-6}$ ,  $1.2 \times 10^{-6}$   
245  $\sim 1.2 \times 10^{-4}$ ,  $1.2 \times 10^{-6} \sim 3.0 \times 10^{-4}$  and  $1.2 \times 10^{-6} \sim 1.8 \times 10^{-4} \text{ s}^{-1}$ , respectively (Jenkin et al.,  
246 1997) (Table S1). The lowest and highest values of these photolysis frequencies were  
247 separately used to determine the lower and upper limits of  $P(RO_x)$ . Therefore, the  
248 total  $P(RO_x)$  contributed by all these OVOC species could be investigated.

## 250 **3 Results and discussion**

### 251 **3.1 Overview of the observations**

252 During the observation period, we used PTR-ToF-MS and GC-MS technology to

253 measure more than 20 photodegradable OVOCs species. The concentrations and  
254 photolysis frequencies of measured photodegradable OVOCs species are summarized  
255 in **Table S1 and Figure 1**. Previous studies have reported that these species have  
256 relatively large absorption cross section and quantum yield (Burkholder et al., 2020).  
257 The measured daytime average photolysis frequencies for these species were generally  
258 larger than  $1.3 \times 10^{-6} \text{ s}^{-1}$ .

259 **Figure 1** presents the average diurnal variation of photodegradable OVOCs  
260 species during the measurement period. The concentrations of these species ranged  
261 from 0.01 to 10 ppb. HCHO, methylglyoxal, propionaldehyde, n-butanal, n-pentanal,  
262 MVK+MACR, pyruvic acid, formic acid, acetic acid, and CH<sub>3</sub>OOH had similar diurnal  
263 variation patterns. The concentrations of these species started to increase from about  
264 6:00 in the morning, and peaked at 13:00-16:00, after which the concentrations  
265 gradually decreased. This diurnal variation pattern is a typical secondary production  
266 pattern, and thus we deduce that these species primarily came from secondary  
267 production. Acetaldehyde, acetone and acrolein showed diurnal variations without  
268 significant variations throughout the day, as these species were contributed by both  
269 secondary generation and primary emissions or background contribution (Wu et al.,  
270 2020). It is notable that acrolein, nitrophenol and methylnitrophenol all peaked at 20:00  
271 in the evening, which is likely due to primary emissions e.g. biomass burning due to  
272 wild/agricultural fires (Ye et al., 2021) and vehicle emissions.

273 The ratio of secondary OVOCs to NMHCs can characterize the degree of the  
274 conversion of emitted NMHC to secondary OVOCs through oxidation reactions.  
275 **Figure S2-S4** presents the correlation between daily daytime average of HCHO (and  
276 pyruvic acid) concentration versus OH reactivity from hydrocarbons, i.e.,  
277  $\text{HCHO}/k_{\text{OH}}R_{\text{OH\_NMHC}}$  ratio (and pyruvic acid/ $k_{\text{OH}}R_{\text{OH\_NMHC}}$  ratio) and  $j(\text{NO}_2)$ . Both  
278  $\text{HCHO}/k_{\text{OH}}R_{\text{OH\_NMHC}}$  and pyruvic acid/ $k_{\text{OH}}R_{\text{OH\_NMHC}}$  ratios displayed significant  
279 positive correlation with  $j(\text{NO}_2)$ . These results suggest that the enhancement of the  
280 photolysis rates converted more NMHCs into secondary OVOCs, suggesting the crucial  
281 role of photolysis reactions in the air mass aging and the occurrence of secondary  
282 pollution.

### 283 3.2 Contribution of photolysis reactions to the production of RO<sub>x</sub> radicals

284 The photolysis of O<sub>3</sub>, HONO and OVOCs are the most important contributors to  
285 the production of RO<sub>x</sub> radicals. All observed photodegradable species, including O<sub>3</sub>,  
286 HONO and OVOCs, were constrained in the box model to calculate P(RO<sub>x</sub>). The  
287 simulated total P(RO<sub>x</sub>) contains the contributions from all observed photodegradable  
288 species and several simulated OVOCs that was not measured such as glyoxal. The  
289 calculated P(RO<sub>x</sub>) was basically determined by concentrations of these observed  
290 photodegradable species. Using the possible ranges of photolysis frequencies of  
291 carbonyls with more carbon number that are not possible to assign into specific  
292 individual species, we can obtain the possible widest variation range of P(RO<sub>x</sub>). As  
293 shown in **Figure 2a**, the minimum (solid line) and maximum (dashed line) of P(RO<sub>x</sub>)  
294 calculated during the campaign peaked at 3.6 ppb h<sup>-1</sup> and 5.4 ppb h<sup>-1</sup>, respectively. The  
295 P(RO<sub>x</sub>) determined in this study is very close to those reported in the Autumn 2014 in  
296 Pearl River Delta with peak values of 3 ~ 4 ppb h<sup>-1</sup> (Tan et al., 2019a) and the summer  
297 2014 in Wangdu, Hebei (peak value of 5 ppb h<sup>-1</sup>) (Tan et al., 2017), and lower than  
298 those in the summer 2006 in Beijing (peak value of about 7 ppb h<sup>-1</sup>) (Lu et al., 2013)  
299 and the summer 2006 in Guangzhou (peak value of about 10 ppb h<sup>-1</sup>) (Lu et al., 2012),  
300 and higher than those in the winter of 2016 in Beijing (peak value of about 1 ppb h<sup>-1</sup>)  
301 (Tan et al., 2018) and the winter in the oil and gas basin of Utah, USA (daytime average  
302 value of 0.77 ppb h<sup>-1</sup>) (Edwards et al., 2014). Note that these previous studies mentioned  
303 above usually only measured a few simple carbonyls such as HCHO, acetaldehyde and  
304 acetone and the P(RO<sub>x</sub>) contributed by photolysis of other OVOCs was calculated by  
305 model simulations, which may lead to large uncertainties.

306 For the scenario of minimum OVOCs contribution, HONO contributed the most  
307 to P(RO<sub>x</sub>) (37%), followed by O<sub>3</sub> (20%) and HCHO (20%). The contribution of non-  
308 HCHO OVOCs was 21% (**Figure 2a**). Figure 2b and Figure S5 show the relative  
309 contributions of different non-HCHO OVOC species to P(RO<sub>x</sub>) for the scenarios with  
310 minimum and maximum OVOC contribution, respectively. Ozonolysis of alkenes  
311 played a minor role in P(RO<sub>x</sub>). For the scenario of maximum OVOCs contribution, the

312 contribution of non-HCHO OVOCs increased to 44%. In total, OVOCs contributed 43%  
313 ~ 59% of P(RO<sub>x</sub>), which is higher than previous studies that reported OVOCs  
314 contributed 17%~40% of P(RO<sub>x</sub>) in major cities in China and the US (Tan et al.,  
315 2019a;Tan et al., 2017;Tan et al., 2018;Tan et al., 2019b;Young et al., 2012;Griffith et  
316 al., 2016). ~~which~~ In this study the contribution of OVOCs to P(RO<sub>x</sub>) was higher than  
317 ~~the contribution that~~ of HONO. This is different from previous studies reporting HONO  
318 contributed more to P(RO<sub>x</sub>) than OVOCs in China (Tan et al., 2019a;Tan et al.,  
319 2017;Tan et al., 2018;Tan et al., 2019b). Nevertheless, it is notable that the contributions  
320 of HONO to P(RO<sub>x</sub>) in the early morning were higher than those of OVOCs due to the  
321 accumulation of HONO in nighttime, while OVOCs dominate P(RO<sub>x</sub>) at noon when  
322 photochemistry was most active (**Figure 2a**). Furthermore, those previous studies in  
323 China indicated that HCHO was the dominant contributor to P(RO<sub>x</sub>) among OVOC  
324 species and the contributions of other OVOC species was generally smaller than that of  
325 HCHO (Tan et al., 2019a;Tan et al., 2017;Tan et al., 2018;Tan et al., 2019b). In contrast,  
326 the results of this study suggest that non-HCHO OVOCs have a potential to be a larger  
327 contributor than HCHO and HONO, revealing the importance of non-HCHO OVOCs  
328 in radical production. The difference between this study and previous studies in China  
329 is primarily attributed to more OVOC species measured in this study than previous  
330 studies. The Nevertheless, the existing isomers of carbonyls with more carbons lead to  
331 large uncertainties in the quantification of P(RO<sub>x</sub>) as shown in **Figure 2a**. Therefore,  
332 precise distinction of these isomers in the future is crucial to accurately quantify P(RO<sub>x</sub>).  
333 In addition, absorption cross-section and quantum yield of many photodegradable  
334 OVOC species with large carbon numbers, especially multifunctional species, are not  
335 experimentally determined. As a result, the photolysis frequencies of these species are  
336 not available, which also leads to uncertainties in quantifying P(RO<sub>x</sub>). As  
337 measurements of many organic compounds may not be possible at least in the near  
338 future, construction of parameterization method for photolysis frequencies of  
339 oxygenated VOCs either based on chemical formula or functional groups at isomeric  
340 level will help to reduce this uncertainty in the future. observation-determined P(RO<sub>x</sub>)

341 As a comparison with the ~~observation-determined P(RO<sub>x</sub>)~~ scenario with all

342 observed OVOC species constrained in the box model, P(RO<sub>x</sub>) was also simulated by  
343 the box model without ~~all~~ observed OVOC species constrained. As shown in **Figure 3a**,  
344 the simulation of the box model without ~~all~~ observed OVOC species constrained (blue  
345 line in Figure 3a) underestimated P(RO<sub>x</sub>) significantly compared to ~~observation-~~  
346 ~~determined P(RO<sub>x</sub>)~~the scenario with all observed OVOC species constrained (red lines  
347 in Figure 3a). The underestimation of P(RO<sub>x</sub>) was 16% and 44% when using the lower  
348 and higher limits of OVOCs photolysis frequencies, respectively (red solid line and red  
349 dashed line in **Figure 3a**). In this case, the underestimation of OH and HO<sub>2</sub>  
350 concentrations were 15~38% and 25%~64%, respectively. The underestimation of  
351 P(RO<sub>x</sub>) and radical concentrations was due to the underestimation of photodegradable  
352 OVOCs simulated by the photochemical model (**Table S2**). In general, most  
353 photodegradable OVOCs were underestimated by 10~100% by box model except for  
354 MVK and MACR. The underestimation of photodegradable OVOCs can be caused by  
355 missing primary emissions (McDonald et al., 2018;Karl et al., 2018;Gkatzelis et al.,  
356 2021) or unknown secondary source of these OVOCs species (Bloss et al., 2005;Ji et al.,  
357 2017). Direct flux measurements of VOCs based on the eddy covariance technique  
358 showed that the contribution of typical urban emission sources comprised of a  
359 surprisingly large portion of OVOCs (Karl et al., 2018). In addition, some experimental  
360 studies indicated that MCM mechanism generally underestimated formation of  
361 aldehydes, ketones and phenols from the oxidation of aromatics by OH radical (Bloss  
362 et al., 2005;Ji et al., 2017), suggesting the existence of unknown secondary source of  
363 these OVOCs species. This evidence suggests that it is essential to use ambient  
364 measurements of OVOCs as constraints in models at least until primary and secondary  
365 sources of OVOCs are better understood.

366 Previous studies in Pearl River Delta and North China Plain of China found that  
367 photochemical models significantly underestimated measured concentrations of OH  
368 radicals, indicating the existence of unknown sources of RO<sub>x</sub> radicals in the atmosphere  
369 (Lu et al., 2012;Lu et al., 2013;Tan et al., 2019c;Hofzumahaus et al., 2009;Ma et al.,  
370 2019). For instance, comprehensive measurements in winter in Beijing showed that the  
371 photochemical box model greatly underestimated OH, HO<sub>2</sub> and RO<sub>2</sub> radicals by 50%

372 ~ 12 fold during the pollution periods (Tan et al., 2018;Ma et al., 2019). Through the  
373 budget analysis of the source and sink of radicals, the researchers believed that the  
374 missing P(RO<sub>x</sub>) was the primary cause of the underestimation of HO<sub>2</sub> and RO<sub>2</sub>  
375 concentrations (Tan et al., 2018). Given that most photodegradable OVOCs were not  
376 constrained in box model used in these previous studies of RO<sub>x</sub> radicals, the results of  
377 our study provide a direction for solving this issue regarding underestimated RO<sub>x</sub>  
378 radical concentrations. Therefore, it is imperative to continuously improve  
379 measurement technologies to achieve accurate quantification of more photodegradable  
380 OVOC species, thereby improving our understanding of the issues with respect to the  
381 closure of RO<sub>x</sub> radicals in the atmosphere.

### 382 **3.3 The role of photolysis reactions in ozone pollution**

383 The box model was used to evaluate the effect of the photodegradable OVOCs  
384 species on ozone production rate during the whole campaign. P(O<sub>3</sub>) were simulated  
385 with and without all of measured photodegradable OVOCs species constrained in the  
386 box model, respectively. As shown in **Figure 3b**, compared to the scenario with  
387 observed photodegradable OVOCs species constrained in box model (red lines in  
388 Figure 3b), the scenario without constraining observed OVOCs (blue line in Figure  
389 3b) underestimated peak value of P(O<sub>3</sub>) by 15~38%. The underestimation of P(O<sub>3</sub>)  
390 was due to the underestimation of OVOCs by the box model (**Table S2**).

391 As shown in **Figure 4**, the dependence of daily peak O<sub>3</sub> concentrations on NO<sub>x</sub>  
392 concentrations was calculated by the box model with and without all of measured  
393 photodegradable OVOCs species constrained. The NO<sub>x</sub> concentration level  
394 corresponding to maximum of ozone concentration (NO<sub>x</sub> (O<sub>3</sub> max)) was determined. In  
395 reality, this NO<sub>x</sub> concentration level is the threshold to distinguish between VOC-  
396 limited and NO<sub>x</sub>-limited regimes (Edwards et al., 2014;Womack et al., 2019). Ozone  
397 production is NO<sub>x</sub>-limited if the ambient NO<sub>x</sub> concentration is lower than the  
398 threshold of NO<sub>x</sub>, but is in VOC-limited regime if ambient NO<sub>x</sub> concentration higher  
399 than the threshold of NO<sub>x</sub>. The larger threshold of NO<sub>x</sub> represents higher possibility  
400 of ozone production in NO<sub>x</sub> limited regime. The threshold of NO<sub>x</sub> for the scenario

401 with observed photodegradable OVOCs species constrained is 21%~52% higher than  
402 that without observed photodegradable OVOCs species constrained (**Figure 4**). This  
403 suggests that the box model simulation without constraining OVOCs will  
404 overestimate the VOC-limited degree due to the underestimation of OVOCs, and thus  
405 overestimate the effect of VOCs reduction in reducing ozone pollution, which in turn  
406 may not determine the ozone control strategy correctly. Therefore, it is necessary to  
407 constrain these important photodegradable species in photochemical models to  
408 calculate P(O<sub>3</sub>) level and to diagnose ozone sensitivity regimes accurately.

409 O<sub>3</sub> production rate can be expressed as the product of P(RO<sub>x</sub>) and radical chain  
410 length (ChL) as shown in E3 (Tonnesen and Dennis, 2000).

$$411 \quad P(O_3) = P(RO_x) \times \frac{\text{Rate}(HO_2+NO) + \text{Rate}(RO_2+NO)}{P(RO_x)} = P(RO_x) \times ChL \quad E3$$

412 where Rate (HO<sub>2</sub>+NO) and Rate (RO<sub>2</sub>+NO) represent the reaction rates between HO<sub>2</sub>  
413 and NO and between RO<sub>2</sub> and NO, respectively. ChL characterizes the number of  
414 iterations each RO<sub>x</sub> radical makes prior to termination. It is equal to the ratio between  
415 the radical recycling rate and primary production rate (or equivalently, termination  
416 rate), indicating the efficiency of radical propagation.

417 Two ozone pollution episodes (from 19 September to 27 September and from 30  
418 September to 9 October, respectively) were identified during the campaign from 14  
419 September to 20 November 2018 (**Figure S3S6, Table S3**). The temporal variations of  
420 P(O<sub>3</sub>) and P(RO<sub>x</sub>) overall showed good consistency with those of ozone concentrations  
421 (**Figure S4S7**). ~~P(O<sub>3</sub>) and P(RO<sub>x</sub>) in the two ozone pollution episodes are higher than~~  
422 ~~those in the non-pollution period (Figure 5, Figure S5).~~ P(O<sub>3</sub>) in the two ozone  
423 pollution episodes was a factor of 2.6~2.8 that in the non-pollution period (Figure 5,  
424 Figure S8). P(RO<sub>x</sub>) in the two ozone pollution episodes was a factor of 2.2~2.6 that in  
425 the non-pollution period. ChL in episode 2 was similar to that in non-pollution period,  
426 while ChL for episode 1 was a factor of 1.7 that in non-pollution period (Figure S8).  
427 ~~ChL levels were similar between the ozone pollution episodes and the non-pollution~~  
428 ~~period (Figure S5).~~ Therefore, the substantial increase of P(RO<sub>x</sub>) in ~~the both~~ ozone  
429 pollution episodes played a crucial role in the accelerated ozone production.

430 Furthermore, the ratio of  $P(\text{RO}_x)$  from OVOCs photolysis to total  $P(\text{RO}_x)$  in the two  
431 ozone pollution episodes is higher than that in the non-pollution period, denoting higher  
432 contribution of OVOCs photolysis to  $P(\text{RO}_x)$  in the ozone pollution episodes (**Figure**  
433 **5**). These results indicate that the accelerating production of OVOCs had a significant  
434 positive feedback effect on ozone pollution (Qu et al., 2021). This is broadly consistent  
435 with the wintertime observations in an oil and gas basin in Utah, USA, which found  
436 that a very high VOC to  $\text{NO}_x$  ratio optimized production of secondary OVOCs, leading  
437 to OVOC photolysis as a dominant oxidant source (Edwards et al., 2014).

#### 438 **4 Summary and Conclusion**

439 In summary, comprehensive measurements of photodegradable species advance  
440 our understand of radical sources and ozone production in an urban environment. By  
441 using PTR-ToF-MS in a representative urban environment, a large number of  
442 photodegradable OVOCs were measured. These measurements make it possible to  
443 directly quantify their contribution to  $\text{RO}_x$  radical production. We found that non-  
444 HCHO OVOCs can be a larger contributor to  $P(\text{RO}_x)$  than HCHO and HONO.  
445 Photochemical models without constrained OVOC species will significantly  
446 underestimate  $P(\text{RO}_x)$  and ozone production rates and overestimate the effect of VOCs  
447 reduction in reducing ozone pollution. Therefore, it is important to measure these  
448 photodegradable species and use these observations as constraints to better quantify  
449 radical and ozone production.

450 Thanks to the improvement of technology in the recent years, large number of  
451 OVOCs species in the atmosphere can be measured by the emerging online chemical  
452 ionization mass spectrometers, including PTR-ToF-MS and CIMS. However,  
453 photolysis frequencies of these OVOCs species, especially those with multiple  
454 functional groups, are still not available or difficult to quantify using current existing  
455 information, which poses large uncertainties in the quantification of  $P(\text{RO}_x)$  and ozone  
456 production. Hence, more laboratory studies on photolysis of organic compounds, better



457 parameterization of photolysis frequencies using chemical formula/functional groups,  
458 and measurements of oxygenated VOCs at isomeric level will help to decrease this  
459 uncertainty in the future.

460

#### 461 **Data availability**

462 The observational data [and model code](#) used in this study are available from  
463 corresponding authors upon request (byuan@jnu.edu.cn).

#### 464 **Author contributions**

465 BY, WJW and HS designed the research. WJW and BY prepared the manuscript  
466 with contributions from other authors. WJW performed data analysis with contributions  
467 from YWP, YFC, SXY and FXB. CHW, JPQ, YBH, CMW, CSY, ZLW, BLW, XMW,  
468 WS, WWH, PC, MNZ, JYZ, and MS collected data

#### 469 **Competing interests**

470 The authors declare that they have no known competing financial interests or personal  
471 relationships that could have appeared to influence the work reported in this paper.

472

#### 473 **Acknowledgements**

474 This work was supported by the National Key R&D Plan of China (grant No.  
475 2019YFE0106300), the National Natural Science Foundation of China (grant No.  
476 41877302, 41905111), Guangdong Natural Science Funds for Distinguished Young  
477 Scholar (grant No. 2018B030306037), Key-Area Research and Development Program  
478 of Guangdong Province (grant No. 2019B110206001), Guangdong Soft Science  
479 Research Program (grant No. 2019B101001005), and Guangdong Innovative and  
480 Entrepreneurial Research Team Program (grant No. 2016ZT06N263). This work was  
481 also supported by Special Fund Project for Science and Technology Innovation Strategy  
482 of Guangdong Province (Grant No.2019B121205004).

483

484 **References:**

- 485 Atkinson, R.: Atmospheric chemistry of VOCs and NO<sub>x</sub>, *Atmos. Environ.*, 34, 2063-  
486 2101, 2000.
- 487 Bejan, I., Abd El Aal, Y., Barnes, I., Benter, T., Bohn, B., Wiesen, P., and Kleffmann, J.:  
488 The photolysis of ortho-nitrophenols: a new gas phase source of HONO, *Physical*  
489 *Chemistry Chemical Physics*, 8, 2028-2035, 2006.
- 490 Berges, M. G., and Warneck, P.: Product quantum yields for the 350 nm  
491 photodecomposition of pyruvic acid in air, *Berichte der Bunsengesellschaft für*  
492 *physikalische Chemie*, 96, 413-416, 1992.
- 493 Bloss, C., Wagner, V., Bonzanini, A., Jenkin, M. E., Wirtz, K., Martin-Reviejo, M., and  
494 Pilling, M. J.: Evaluation of detailed aromatic mechanisms (MCMv3 and MCMv3.1)  
495 against environmental chamber data, *Atmos. Chem. Phys.*, 5, 623-639, 10.5194/acp-5-  
496 623-2005, 2005.
- 497 Burkholder, J., Sander, S., Abbatt, J., Barker, J., Cappa, C., Crouse, J., Dibble, T., Huie,  
498 R., Kolb, C., and Kurylo, M.: Chemical kinetics and photochemical data for use in  
499 atmospheric studies; evaluation number 19, Pasadena, CA: Jet Propulsion Laboratory,  
500 National Aeronautics and Space ..., 2020.
- 501 Chen, J., Wenger, J. C., and Venables, D. S.: Near-ultraviolet absorption cross sections  
502 of nitrophenols and their potential influence on tropospheric oxidation capacity, *The*  
503 *Journal of Physical Chemistry A*, 115, 12235-12242, 2011.
- 504 Edwards, P. M., Brown, S. S., Roberts, J. M., Ahmadov, R., Banta, R. M., deGouw, J.  
505 A., Dubé, W. P., Field, R. A., Flynn, J. H., Gilman, J. B., Graus, M., Helmig, D., Koss,  
506 A., Langford, A. O., Lefer, B. L., Lerner, B. M., Li, R., Li, S.-M., McKeen, S. A.,  
507 Murphy, S. M., Parrish, D. D., Senff, C. J., Soltis, J., Stutz, J., Sweeney, C., Thompson,  
508 C. R., Trainer, M. K., Tsai, C., Veres, P. R., Washenfelder, R. A., Warneke, C., Wild, R.  
509 J., Young, C. J., Yuan, B., and Zamora, R.: High winter ozone pollution from carbonyl  
510 photolysis in an oil and gas basin, *Nature*, 514, 351-354, 10.1038/nature13767, 2014.
- 511 Ehhalt, D. H., and Rohrer, F.: Dependence of the OH concentration on solar UV, *J.*  
512 *Geophys. Res.-Atmos.*, 105, 3565-3571, 10.1029/1999jd901070, 2000.
- 513 Emmerson, K. M., Carslaw, N., Carpenter, L. J., Heard, D. E., Lee, J. D., and Pilling,  
514 M. J.: Urban Atmospheric Chemistry During the PUMA Campaign 1: Comparison of  
515 Modelled OH and HO<sub>2</sub> Concentrations with Measurements, *Journal of Atmospheric*  
516 *Chemistry*, 52, 143-164, 10.1007/s10874-005-1322-3, 2005.
- 517 Gkatzelis, G. I., Coggon, M. M., McDonald, B. C., Peischl, J., Gilman, J. B., Aikin, K.  
518 C., Robinson, M. A., Canonaco, F., Prevot, A. S., and Trainer, M.: Observations confirm  
519 that volatile chemical products are a major source of petrochemical emissions in US  
520 cities, *Environmental science & technology*, 55, 4332-4343, 2021.
- 521 Griffith, S. M., Hansen, R., Dusanter, S., Michoud, V., Gilman, J., Kuster, W., Veres, P.,  
522 Graus, M., de Gouw, J., and Roberts, J.: Measurements of hydroxyl and hydroperoxy  
523 radicals during CalNex-LA: Model comparisons and radical budgets, *Journal of*  
524 *Geophysical Research: Atmospheres*, 121, 4211-4232, 2016.
- 525 Hofzumahaus, A., Rohrer, F., Lu, K., Bohn, B., Brauers, T., Chang, C.-C., Fuchs, H.,  
526 Holland, F., Kita, K., and Kondo, Y.: Amplified trace gas removal in the troposphere,

527 Science, 324, 1702-1704, 2009.

528 Horowitz, A., Meller, R., and Moortgat, G. K.: The UV–VIS absorption cross sections  
529 of the  $\alpha$ -dicarbonyl compounds: pyruvic acid, biacetyl and glyoxal, *Journal of*  
530 *Photochemistry and Photobiology A: Chemistry*, 146, 19-27, 2001.

531 Jenkin, M. E., Saunders, S. M., and Pilling, M. J.: The tropospheric degradation of  
532 volatile organic compounds: a protocol for mechanism development, *Atmos. Environ.*,  
533 31, 81-104, 1997.

534 Jenkin, M. E., Saunders, S. M., Wagner, V., and Pilling, M. J.: Protocol for the  
535 development of the Master Chemical Mechanism, MCM v3 (Part B): tropospheric  
536 degradation of aromatic volatile organic compounds, *Atmospheric Chemistry and*  
537 *Physics*, 3, 181-193, 10.5194/acp-3-181-2003, 2003.

538 Ji, Y., Zhao, J., Terazono, H., Misawa, K., Levitt, N. P., Li, Y., Lin, Y., Peng, J., Wang,  
539 Y., Duan, L., Pan, B., Zhang, F., Feng, X., An, T., Marrero-Ortiz, W., Secret, J., Zhang,  
540 A. L., Shibuya, K., Molina, M. J., and Zhang, R.: Reassessing the atmospheric oxidation  
541 mechanism of toluene, *Proceedings of the National Academy of Sciences*, 114, 8169-  
542 8174, 10.1073/pnas.1705463114, 2017.

543 Karl, T., Striednig, M., Graus, M., Hammerle, A., and Wohlfahrt, G.: Urban flux  
544 measurements reveal a large pool of oxygenated volatile organic compound emissions,  
545 *Proceedings of the National Academy of Sciences*, 115, 1186-1191, 2018.

546 Lelieveld, J., Butler, T. M., Crowley, J. N., Dillon, T. J., Fischer, H., Ganzeveld, L.,  
547 Harder, H., Lawrence, M. G., Martinez, M., Taraborrelli, D., and Williams, J.:  
548 Atmospheric oxidation capacity sustained by a tropical forest, *Nature*, 452, 737-740,  
549 10.1038/nature06870, 2008.

550 Li, K., Jacob, D. J., Liao, H., Qiu, Y., Shen, L., Zhai, S., Bates, K. H., Sulprizio, M. P.,  
551 Song, S., and Lu, X.: Ozone pollution in the North China Plain spreading into the late-  
552 winter haze season, *Proceedings of the National Academy of Sciences*, 118, 2021.

553 Li, X., Rohrer, F., Brauers, T., Hofzumahaus, A., Lu, K., Shao, M., Zhang, Y. H., and  
554 Wahner, A.: Modeling of HCHO and CHOCHO at a semi-rural site in southern China  
555 during the PRIDE-PRD2006 campaign, *Atmos. Chem. Phys.*, 14, 12291-12305,  
556 10.5194/acp-14-12291-2014, 2014.

557 Ling, Z., Guo, H., Lam, S., Saunders, S., and Wang, T.: Atmospheric photochemical  
558 reactivity and ozone production at two sites in Hong Kong: Application of a master  
559 chemical mechanism–photochemical box model, *Journal of Geophysical Research:*  
560 *Atmospheres*, 119, 10567-10582, 2014.

561 Lu, K., Rohrer, F., Holland, F., Fuchs, H., Bohn, B., Brauers, T., Chang, C., Häsel, R.,  
562 Hu, M., and Kita, K.: Observation and modelling of OH and HO<sub>2</sub> concentrations in the  
563 Pearl River Delta 2006: a missing OH source in a VOC rich atmosphere, *Atmospheric*  
564 *chemistry and physics*, 12, 1541, 2012.

565 Lu, K. D., Hofzumahaus, A., Holland, F., Bohn, B., Brauers, T., Fuchs, H., Hu, M.,  
566 Haseler, R., Kita, K., Kondo, Y., Li, X., Lou, S. R., Oebel, A., Shao, M., Zeng, L. M.,  
567 Wahner, A., Zhu, T., Zhang, Y. H., and Rohrer, F.: Missing OH source in a suburban  
568 environment near Beijing: observed and modelled OH and HO<sub>2</sub> concentrations in  
569 summer 2006, *Atmospheric Chemistry and Physics*, 13, 1057-1080, 10.5194/acp-13-  
570 1057-2013, 2013.

571 Ma, X., Tan, Z., Lu, K., Yang, X., Liu, Y., Li, S., Li, X., Chen, S., Novelli, A., and Cho,  
572 C.: Winter photochemistry in Beijing: Observation and model simulation of OH and  
573 HO<sub>2</sub> radicals at an urban site, *Science of the Total Environment*, 685, 85-95, 2019.

574 McDonald, B. C., De Gouw, J. A., Gilman, J. B., Jathar, S. H., Akherati, A., Cappa, C.  
575 D., Jimenez, J. L., Lee-Taylor, J., Hayes, P. L., and McKeen, S. A.: Volatile chemical  
576 products emerging as largest petrochemical source of urban organic emissions, *Science*,  
577 359, 760-764, 2018.

578 Mellouki, A., and Mu, Y.: On the atmospheric degradation of pyruvic acid in the gas  
579 phase, *Journal of Photochemistry and Photobiology A: Chemistry*, 157, 295-300, 2003.

580 Monks, P. S., Archibald, A., Colette, A., Cooper, O., Coyle, M., Derwent, R., Fowler,  
581 D., Granier, C., Law, K. S., and Mills, G.: Tropospheric ozone and its precursors from  
582 the urban to the global scale from air quality to short-lived climate forcer, *Atmospheric  
583 Chemistry and Physics*, 15, 8889-8973, 2015.

584 Qu, H., Wang, Y., Zhang, R., Liu, X., Huey, L. G., Sjostedt, S., Zeng, L., Lu, K., Wu,  
585 Y., and Shao, M.: Chemical Production of Oxygenated Volatile Organic Compounds  
586 Strongly Enhances Boundary-Layer Oxidation Chemistry and Ozone Production,  
587 *Environmental Science & Technology*, 55, 13718-13727, 2021.

588 Rohrer, F., Lu, K., Hofzumahaus, A., Bohn, B., Brauers, T., Chang, C.-C., Fuchs, H.,  
589 Häsel, R., Holland, F., and Hu, M.: Maximum efficiency in the hydroxyl-radical-  
590 based self-cleansing of the troposphere, *Nature Geoscience*, 7, 559-563, 2014a.

591 Rohrer, F., Lu, K., Hofzumahaus, A., Bohn, B., Brauers, T., Chang, C.-C., Fuchs, H.,  
592 Häsel, R., Holland, F., Hu, M., Kita, K., Kondo, Y., Li, X., Lou, S., Oebel, A., Shao,  
593 M., Zeng, L., Zhu, T., Zhang, Y., and Wahner, A.: Maximum efficiency in the hydroxyl-  
594 radical-based self-cleansing of the troposphere, *Nature Geoscience*, 7, 559-563,  
595 10.1038/ngeo2199, 2014b.

596 Sangwan, M., and Zhu, L.: Role of methyl-2-nitrophenol photolysis as a potential  
597 source of OH radicals in the polluted atmosphere: implications from laboratory  
598 investigation, *The Journal of Physical Chemistry A*, 122, 1861-1872, 2018.

599 Saunders, S. M., Jenkin, M. E., Derwent, R., and Pilling, M.: Protocol for the  
600 development of the Master Chemical Mechanism, MCM v3 (Part A): tropospheric  
601 degradation of non-aromatic volatile organic compounds, 2003.

602 Sekimoto, K., Li, S.-M., Yuan, B., Koss, A., Coggon, M., Warneke, C., and de Gouw,  
603 J.: Calculation of the sensitivity of proton-transfer-reaction mass spectrometry (PTR-  
604 MS) for organic trace gases using molecular properties, *International Journal of Mass  
605 Spectrometry*, 421, 71-94, 10.1016/j.ijms.2017.04.006, 2017.

606 Sheehy, P. M., Volkamer, R., Molina, L. T., and Molina, M. J.: Oxidative capacity of  
607 the Mexico City atmosphere - Part 2: A RO<sub>x</sub> radical cycling perspective, *Atmospheric  
608 Chemistry and Physics*, 10, 6993-7008, 10.5194/acp-10-6993-2010, 2010.

609 Sinha, V., Williams, J., Crowley, J. N., and Lelieveld, J.: The Comparative Reactivity  
610 Method &ndash; a new tool to measure total OH Reactivity in ambient air, *Atmos.  
611 Chem. Phys.*, 8, 2213-2227, 10.5194/acp-8-2213-2008, 2008.

612 Stone, D., Whalley, L. K., and Heard, D. E.: Tropospheric OH and HO<sub>2</sub> radicals: field  
613 measurements and model comparisons, *Chem. Soc. Rev.*, 41, 6348-6404,  
614 10.1039/c2cs35140d, 2012.

615 Tan, Z., Fuchs, H., Lu, K., Hofzumahaus, A., Bohn, B., Broch, S., Dong, H., Gomm, S.,  
616 Häsel, R., He, L., Holland, F., Li, X., Liu, Y., Lu, S., Rohrer, F., Shao, M., Wang, B.,  
617 Wang, M., Wu, Y., Zeng, L., Zhang, Y., Wahner, A., and Zhang, Y.: Radical chemistry  
618 at a rural site (Wangdu) in the North China Plain: observation and model calculations  
619 of OH, HO<sub>2</sub> and RO<sub>2</sub> radicals, *Atmos. Chem. Phys.*, 17, 663-690, 10.5194/acp-17-663-  
620 2017, 2017.

621 Tan, Z., Rohrer, F., Lu, K., Ma, X., Bohn, B., Broch, S., Dong, H., Fuchs, H., Gkatzelis,  
622 G. I., Hofzumahaus, A., Holland, F., Li, X., Liu, Y., Liu, Y., Novelli, A., Shao, M., Wang,  
623 H., Wu, Y., Zeng, L., Hu, M., Kiendler-Scharr, A., Wahner, A., and Zhang, Y.:  
624 Wintertime photochemistry in Beijing: observations of RO<sub>x</sub> radical concentrations in  
625 the North China Plain during the BEST-ONE campaign, *Atmos. Chem. Phys.*, 18,  
626 12391-12411, 10.5194/acp-18-12391-2018, 2018.

627 Tan, Z., Lu, K., Hofzumahaus, A., Fuchs, H., Bohn, B., Holland, F., Liu, Y., Rohrer, F.,  
628 Shao, M., and Sun, K.: Experimental budgets of OH, HO<sub>2</sub>, and RO<sub>2</sub> radicals and  
629 implications for ozone formation in the Pearl River Delta in China 2014, *Atmospheric  
630 chemistry and physics*, 19, 7129-7150, 2019a.

631 Tan, Z., Lu, K., Jiang, M., Su, R., Wang, H., Lou, S., Fu, Q., Zhai, C., Tan, Q., Yue, D.,  
632 Chen, D., Wang, Z., Xie, S., Zeng, L., and Zhang, Y.: Daytime atmospheric oxidation  
633 capacity in four Chinese megacities during the photochemically polluted season: a case  
634 study based on box model simulation, *Atmos. Chem. Phys.*, 19, 3493-3513,  
635 10.5194/acp-19-3493-2019, 2019b.

636 Tan, Z. F., Lu, K. D., Hofzumahaus, A., Fuchs, H., Bohn, B., Holland, F., Liu, Y. H.,  
637 Rohrer, F., Shao, M., Sun, K., Wu, Y. S., Zeng, L. M., Zhang, Y. S., Zou, Q., Kiendler-  
638 Scharr, A., Wahner, A., and Zhang, Y. H.: Experimental budgets of OH, HO<sub>2</sub>, and RO<sub>2</sub>  
639 radicals and implications for ozone formation in the Pearl River Delta in China 2014,  
640 *Atmospheric Chemistry and Physics*, 19, 7129-7150, 10.5194/acp-19-7129-2019,  
641 2019c.

642 Tonnesen, G. S., and Dennis, R. L.: Analysis of radical propagation efficiency to assess  
643 ozone sensitivity to hydrocarbons and NO<sub>x</sub>: 1. Local indicators of instantaneous odd  
644 oxygen production sensitivity, *Journal of Geophysical Research: Atmospheres*, 105,  
645 9213-9225, 2000.

646 Volkamer, R., Sheehy, P., Molina, L. T., and Molina, M. J.: Oxidative capacity of the  
647 Mexico City atmosphere - Part 1: A radical source perspective, *Atmospheric Chemistry  
648 and Physics*, 10, 6969-6991, 10.5194/acp-10-6969-2010, 2010.

649 Wang, C., Yuan, B., Wu, C., Wang, S., Qi, J., Wang, B., Wang, Z., Hu, W., Chen, W.,  
650 Ye, C., Wang, W., Sun, Y., Wang, C., Huang, S., Song, W., Wang, X., Yang, S., Zhang,  
651 S., Xu, W., Ma, N., Zhang, Z., Jiang, B., Su, H., Cheng, Y., Wang, X., and Shao, M.:  
652 Measurements of higher alkanes using NO<sup>+</sup> chemical ionization in PTR-ToF-MS:  
653 important contributions of higher alkanes to secondary organic aerosols in China,  
654 *Atmospheric Chemistry and Physics*, 20, 14123-14138, 10.5194/acp-20-14123-2020,  
655 2020a.

656 Wang, W., Parrish, D. D. P., Li, X., Shao, M., Liu, Y., Lu, S., Hu, M., Wu, Y., Zeng, L.,  
657 and Zhang, Y.: Exploring the drivers of the elevated ozone production in Beijing in  
658 summertime during 2005–2016, *Atmospheric Chemistry and Physics Discussions*, 1-

659 40, 2020b.

660 Wang, W., Qi, J., Zhou, J., Yuan, B., Peng, Y., Wang, S., Yang, S., Williams, J., Sinha,  
661 V., and Shao, M.: The improved comparative reactivity method (ICRM): measurements  
662 of OH reactivity under high-NO<sub>x</sub> conditions in ambient air, *Atmos. Meas. Tech.*, 14,  
663 2285-2298, 2021.

664 Womack, C. C., McDuffie, E. E., Edwards, P. M., Bares, R., de Gouw, J. A., Docherty,  
665 K. S., Dubé, W. P., Fibiger, D. L., Franchin, A., Gilman, J. B., Goldberger, L., Lee, B.  
666 H., Lin, J. C., Long, R., Middlebrook, A. M., Millet, D. B., Moravek, A., Murphy, J. G.,  
667 Quinn, P. K., Riedel, T. P., Roberts, J. M., Thornton, J. A., Valin, L. C., Veres, P. R.,  
668 Whitehill, A. R., Wild, R. J., Warneke, C., Yuan, B., Baasandorj, M., and Brown, S. S.:  
669 An Odd Oxygen Framework for Wintertime Ammonium Nitrate Aerosol Pollution in  
670 Urban Areas: NO<sub>x</sub> and VOC Control as Mitigation Strategies, *Geophys. Res. Lett.*, 46,  
671 4971-4979, 10.1029/2019gl082028, 2019.

672 Wu, C., Wang, C., Wang, S., Wang, W., Yuan, B., Qi, J., Wang, B., Wang, H., Wang, C.,  
673 Song, W., Wang, X., Hu, W., Lou, S., Ye, C., Peng, Y., Wang, Z., Huangfu, Y., Xie, Y.,  
674 Zhu, M., Zheng, J., Wang, X., Jiang, B., Zhang, Z., and Shao, M.: Measurement report:  
675 Important contributions of oxygenated compounds to emissions and chemistry of  
676 volatile organic compounds in urban air, *Atmospheric Chemistry and Physics*, 20,  
677 14769-14785, 10.5194/acp-20-14769-2020, 2020.

678 Ye, C., Yuan, B., Lin, Y., Wang, Z., Hu, W., Li, T., Chen, W., Wu, C., Wang, C., Huang,  
679 S., Qi, J., Wang, B., Wang, C., Song, W., Wang, X., Zheng, E., Krechmer, J. E., Ye, P.,  
680 Zhang, Z., Wang, X., Worsnop, D. R., and Shao, M.: Chemical characterization of  
681 oxygenated organic compounds in the gas phase and particle phase using iodide CIMS  
682 with FIGAERO in urban air, *Atmospheric Chemistry and Physics*, 21, 8455-8478,  
683 10.5194/acp-21-8455-2021, 2021.

684 Young, C. J., Washenfelder, R. A., Roberts, J. M., Mielke, L. H., Osthoff, H. D., Tsai,  
685 C., Pikelnaya, O., Stutz, J., Veres, P. R., and Cochran, A. K.: Vertically resolved  
686 measurements of nighttime radical reservoirs in Los Angeles and their contribution to  
687 the urban radical budget, *Environmental science & technology*, 46, 10965-10973, 2012.

688 Yu, Y., Cheng, P., Li, H., Yang, W., Han, B., Song, W., Hu, W., Wang, X., Yuan, B.,  
689 Shao, M., Huang, Z., Li, Z., Zheng, J., Wang, H., and Yu, X.: Budget of nitrous acid  
690 (HONO) and its impacts on atmospheric oxidation capacity at an urban site in the fall  
691 season of Guangzhou, China, *Atmos. Chem. Phys. Discuss.*, 2021, 1-38, 10.5194/acp-  
692 2021-178, 2021.

693 Yuan, B., Liggio, J., Wentzell, J., Li, S. M., Stark, H., Roberts, J. M., Gilman, J., Lerner,  
694 B., Warneke, C., Li, R., Leithead, A., Osthoff, H. D., Wild, R., Brown, S. S., and de  
695 Gouw, J. A.: Secondary formation of nitrated phenols: insights from observations  
696 during the Uintah Basin Winter Ozone Study (UBWOS) 2014, *Atmos. Chem. Phys.*, 16,  
697 2139-2153, 10.5194/acp-16-2139-2016, 2016.

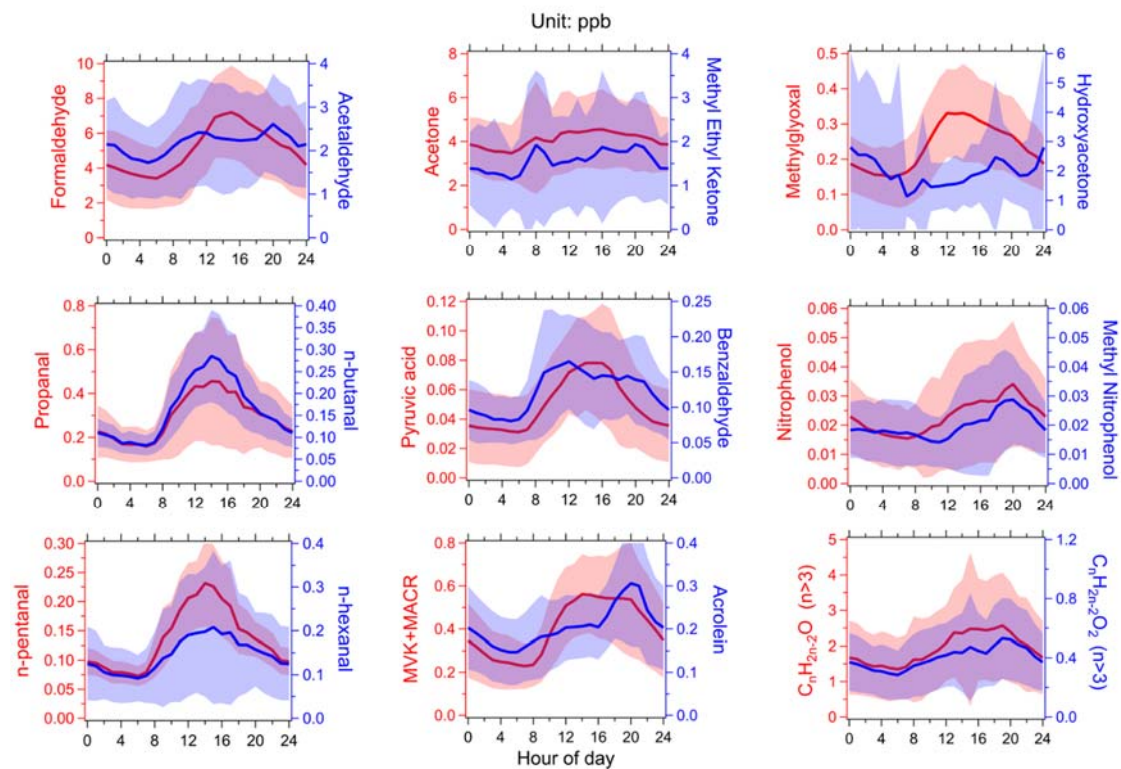
698 Yuan, B., Koss, A. R., Warneke, C., Coggon, M., Sekimoto, K., and de Gouw, J. A.:  
699 Proton-Transfer-Reaction Mass Spectrometry: Applications in Atmospheric Sciences,  
700 *Chem. Rev.*, 117, 13187-13229, 10.1021/acs.chemrev.7b00325, 2017.

701

702

703

704



705

706

Figure 1. The average diurnal variations of the concentrations of photodegradable

707

OVOCs species during the field campaign in Guangzhou. Lines and shading represent

708

averages and standard deviations, respectively.

709

710



711  
 712  
 713  
 714  
 715  
 716  
 717  
 718  
 719  
 720  
 721  
 722  
 723  
 724  
 725  
 726  
 727  
 728  
 729  
 730  
 731  
 732  
 733  
 734  
 735  
 736  
 737  
 738  
 739  
 740

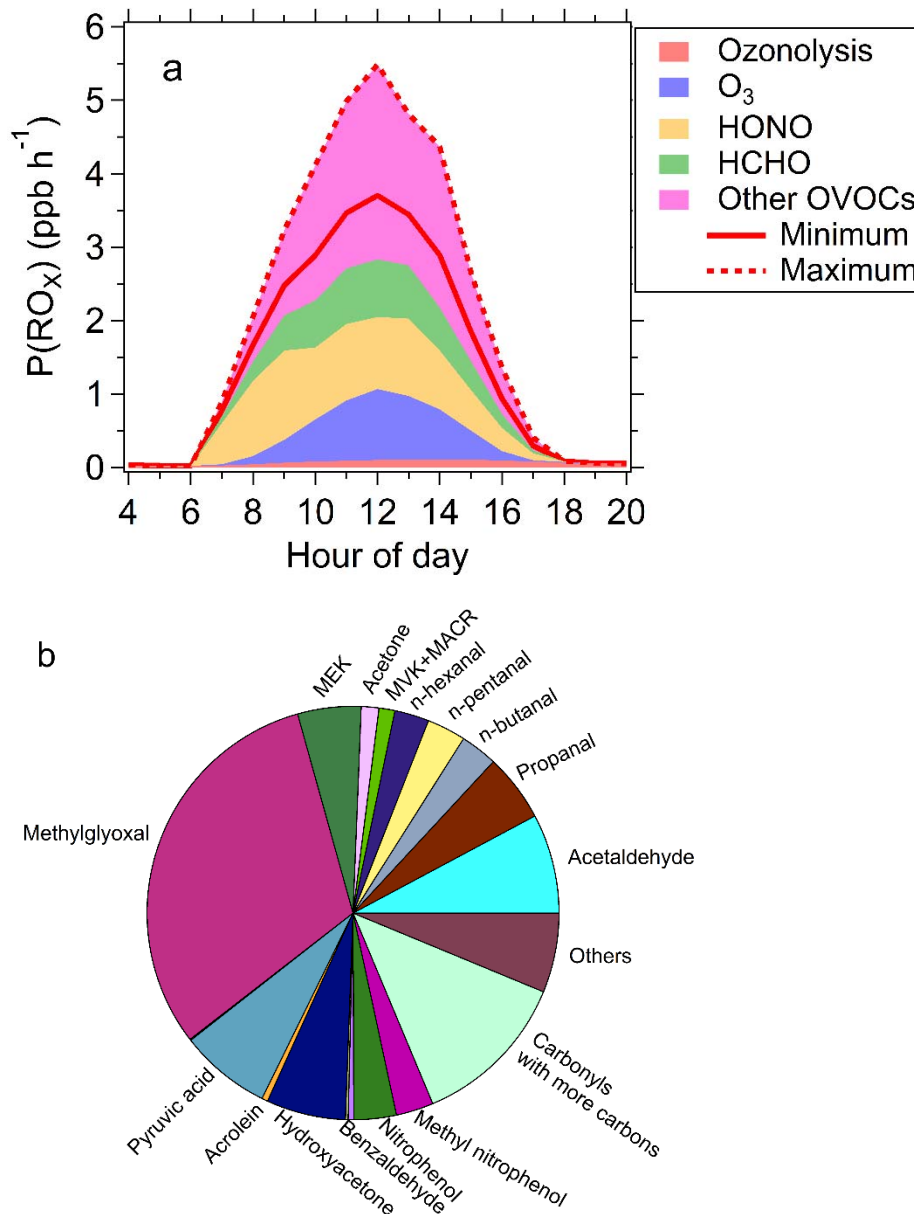


Figure 2. The P(RO<sub>x</sub>) calculated by box model with all observed photodegradable species constrained. (a): The source composition of total P(RO<sub>x</sub>) during the campaign; the solid and dashed lines represent the scenarios with minimum and maximum OVOC contributions to P(RO<sub>x</sub>), respectively. (b): the relative contributions of non-HCHO OVOC species to P(RO<sub>x</sub>) for the scenarios with minimum OVOC contribution to P(RO<sub>x</sub>).

741  
742  
743  
744  
745  
746  
747  
748  
749  
750  
751  
752  
753  
754  
755  
756  
757  
758  
759  
760  
761  
762

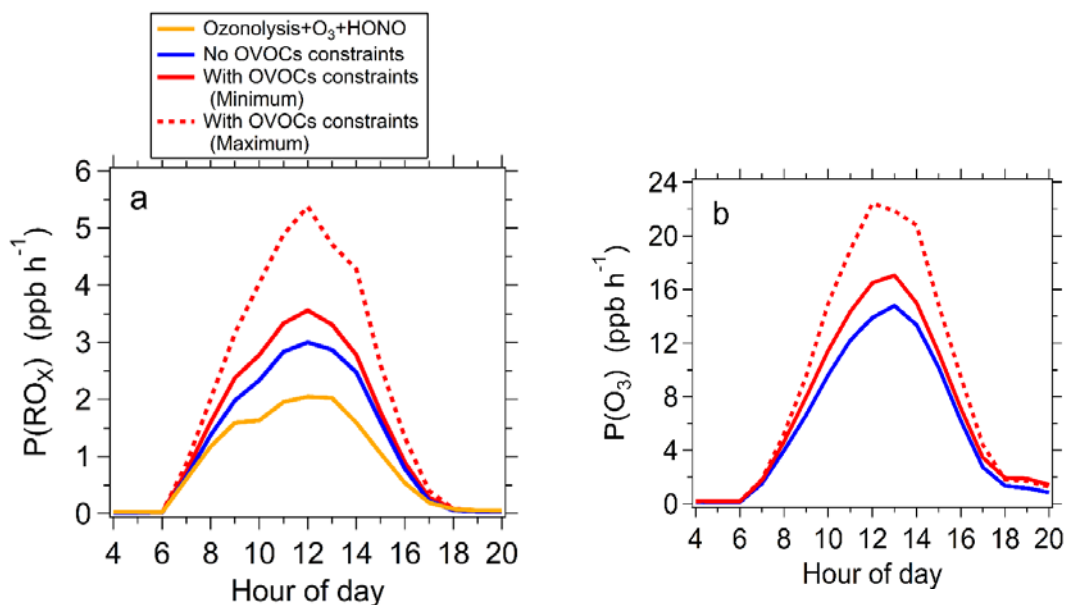
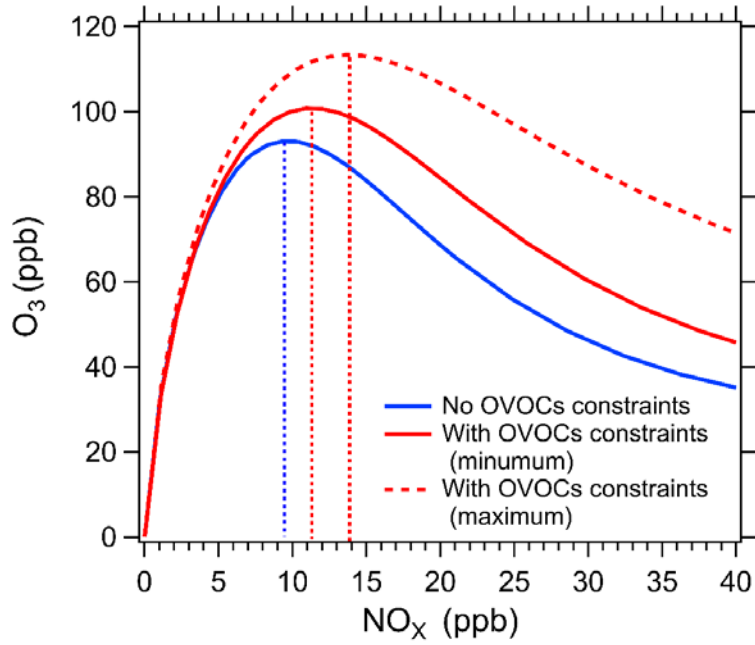


Figure 3. Model simulated  $P(\text{RO}_x)$  (a) and  $P(\text{O}_3)$  (b) without and with all observed photodegradable OVOCs constrained. (a): Model simulated  $P(\text{RO}_x)$  without (blue line) and with all observed photodegradable OVOCs constrained (red lines). The sum contribution of  $\text{O}_3$  photolysis, HONO photolysis and ozonolysis is also displayed (yellow line). (b): Model simulated  $P(\text{O}_3)$  without (blue line) and with observed photodegradable OVOCs constrained (red lines). The red solid and red dashed lines represent the scenarios with minimum and maximum OVOC contributions to  $P(\text{RO}_x)$ , respectively.



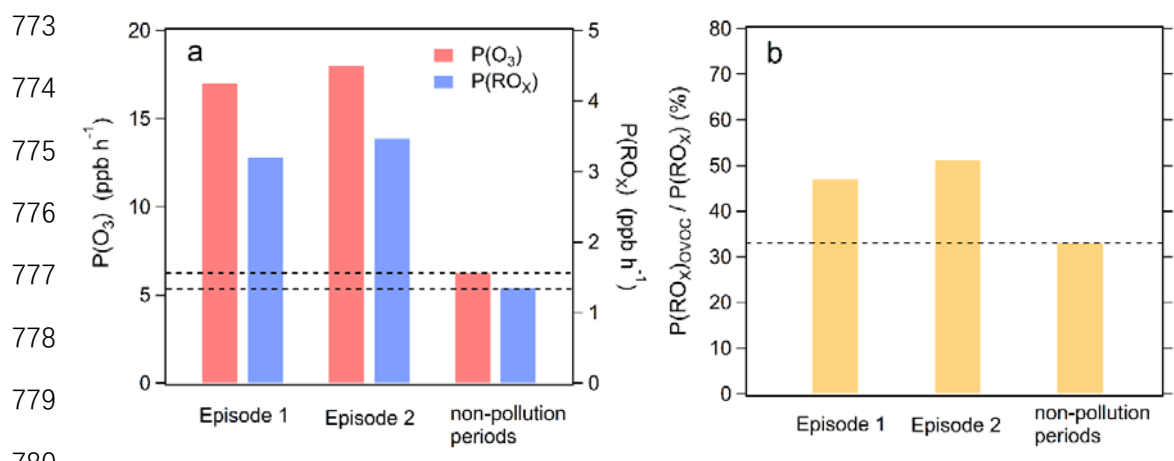
763

764 Figure 4. Model simulated dependence of daily peak O<sub>3</sub> concentrations on NO<sub>x</sub>  
 765 concentrations without (blue curve) and with all observed photodegradable OVOCs  
 766 constrained (red curves). The red solid and red dashed curves represent the scenarios  
 767 with minimum and maximum OVOC contributions to P(RO<sub>x</sub>), respectively. The dashed  
 768 lines parallel to Y-axis represent the threshold of NO<sub>x</sub> levels to distinguish between  
 769 VOC-limited and NO<sub>x</sub>-limited regimes.

770

771

772



781 Figure 5. Averaged  $P(O_3)$ ,  $P(RO_x)$ , the ratio of  $P(RO_x)$  contributed by OVOCs to total  
 782  $P(RO_x)$  ( $P(RO_x)_{OVOC}/P(RO_x)$ ) during two ozone pollution episodes (episode 1,  
 783 episode 2) and non-pollution periods. Both  $P(O_3)$  and  $P(RO_x)$  correspond to the  
 784 scenarios with minimum OVOC contributions to  $P(RO_x)$ .

785  
 786  
 787